ACS APPLIED OPTICAL MATERIALS

pubs.acs.org/acsaom

Forum Article

Improving Accuracy and Sensitivity of Lanthanide-Based Luminescent Manometers by Augmented Spectral Shift Method

M. Pieprz, M. Runowski, K. Ledwa, J. J. Carvajal, A. Bednarkiewicz, and L. Marciniak*

Cite This: https://doi.org/10.1021/acsaom.2c00198

Read Online

ACCESS | Metrics & More | Article Recommendations | Supporting Information

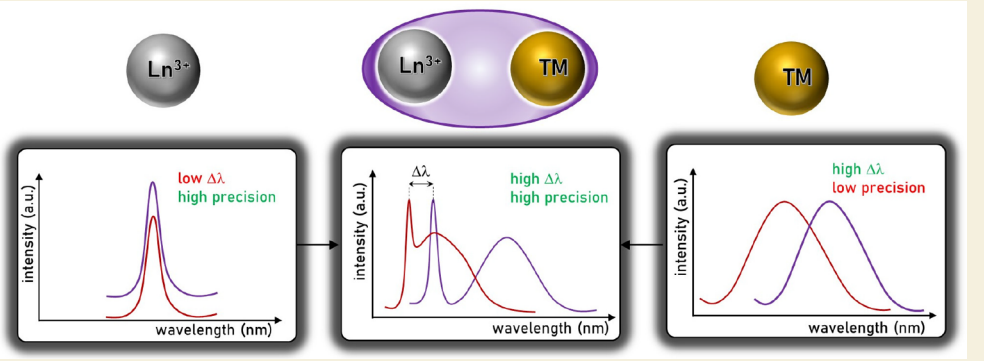

ABSTRACT: Luminescence manometry is most often realized by a spectral shift of luminescence bands. Typically, the shift of spectrally narrow-band emission is quantified, which is highly precise but not very sensitive to pressure variations. Alternatively, the spectral shift of a broadband emission may be exploited, which is more sensitive but less precise, due to the difficulty in accurate determination of the band centroid. In this work, a mixed approach is presented, combining the shift in broadband chromium emission from the $^4T_2 \rightarrow {}^4A_2$ level with a narrow-band neodymium emission ($^4F_{3/2} \rightarrow {}^4I_{11/2}$ transition), observed in the $La_3Ga_5GeO_{14}$ spectrum. The resulting optical Nd^{3+}-based manometer demonstrates an absolute sensitivity of 2.92 cm^{-1}/GPa for the $^4F_{3/2} \rightarrow {}^4I_{11/2}$ electronic transition. An additional advantage of using this material is its negligible spectral shift with temperature, determined in the T range of 77−343 K, making the pressure readouts independent of this parameter (i.e., temperature variations).

KEYWORDS: *luminescent manometer, pressure sensor, Cr^{3+}, crystal field strength, luminescence intensity ratio, manometry*

INTRODUCTION

The remote pressure measurements offered by luminescent manometer phosphors are crucial for enabling the technology of numerous new diagnostic fields, which were unavailable to any previous pressure-monitoring techniques.[1−13] The use of a pressure-dependent luminescence band shift, changes in luminescence kinetics, or the ratio of the intensity of two luminophore emission bands do not require electrical connections between the sensor and the sensing system.[2,14,15] This is especially important in a pressure chamber of the diamond anvil cell (DAC), microfluidic systems, or even biological systems.[16−19] One of the most popular and widely used luminescent pressure indicators is ruby, Al_2O_3:Cr^{3+}.[20] In this case, an increase in pressure leads to an increase in the covalence of the Cr^{3+}−O^{2-} bond and a decrease in the Racah parameter. Thus, the narrow emission band associated with the $^2E_g \rightarrow {}^4A_{2g}$ electron transition is spectrally shifted upon compression. The spectrally narrow nature of this band provides high-precision pressure readouts. In addition, the applicability of this material over a very wide range of pressures, i.e., up to ∼150 GPa, has been confirmed experimentally.[21−24] However, a limitation of this pressure sensor is its relatively small spectral shift with the applied pressure (∼0.35 nm/GPa). In addition, the fact that this band is located at ∼694 nm often makes luminescence measurements difficult or impossible due to the spectral overlap between the signal of the pressure sensor and the luminescence signal from the investigated material. Moreover, the emission of ruby is strongly temperature-dependent ($d\lambda/dT \approx 0.007$ nm/K), hampering high-pressure experiments performed under varied temperature conditions. An alternative approach to the narrow-band luminescence manometers is to use spectrally broadband luminophores based, e.g., on the luminescence of Ce^{3+},[25] Eu^{2+},[26,27] or Tm^{2+}[28] ions or transition metal ions.[3,29,30] However, the broad Gaussian-like emission

Special Issue: Phosphors for Infrared Applications

Received: December 27, 2022
Accepted: February 28, 2023

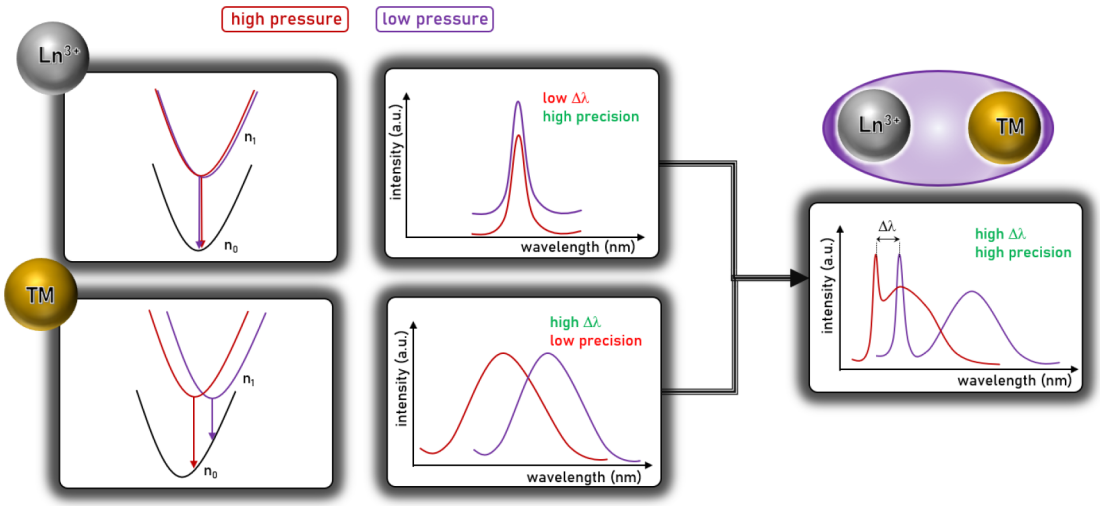

Figure 1. Schematic representation of the concept of the manuscript. The codoping of Ln^{3+} ions characterized by a small pressure-induced spectral shift of the emission band with the TM of a large pressure-induced spectral shift enables the development of modern optical manometers with good precision and sensitivity of pressure readouts.

band limits the ability of accurate determination of the band maximum and its centroid and deteriorates the precision of the measurement. Therefore, it is necessary to search for other luminescent manometers that offer (I) both high precision and sensitivity; (II) temperature-independence; and (III) a different emission spectral range in order to get rid of the interference from the surroundings (DAC assembly). In response to this demand, in this work we propose an approach that allows for sensitizing the emission of lanthanide ions (Ln^{3+}) to pressure changes by material codoping with transition metal (TM) ions. The mentioned idea is schematically depicted in Figure 1. As is well-known, the luminescence of Ln^{3+} ions is predominantly realized through 4f−4f type electron transitions. Due to the weak electron−phonon coupling observed in that case, as well as the shielding of the 4f orbitals from the environment by the 5s and 5p orbitals, the applied pressure has only a small effect on the spectral position of the narrow Ln^{3+} luminescence bands. On the other hand, in the case of transition metal ions, even a relatively low pressure significantly affects the crystal field strength by changing the spectral position of the corresponding TM band. The proposed solution is based on the fact that, in the case of spectral overlap between the TM and Ln^{3+} bands, the narrow Ln^{3+} band apparently shifts spectrally with the applied pressure. This is due to the integration of the luminescence originating from the TM and Ln^{3+} signals. It makes it possible to mimic a pressure shift of the Ln^{3+} band and thus sensitize the Ln^{3+} luminescence to pressure changes. As shown by the simulations performed in this work, this is a universal approach that makes it possible, through the appropriate selection of TMs, to achieve a similar effect for any Ln^{3+}. Thanks to its application, the emission range of optical pressure indicators, operating from UV through VIS to NIR, can be extended. The good accuracy of the band maximum readout, originating from spectrally narrow 4f−4f bands, provides a precision of pressure sensing comparable to that of ruby. In addition, the more spectrally broad are the TM bands, the higher is the absorption cross section of the TM ion, so the TM → Ln^{3+} energy transfer allow us to broaden the spectral range, enabling excitation of the pressure indicator (Ln^{3+}) and increasing its emission intensity. We believe that thanks to the versatility and simplicity of the proposed solution, it will extend the available spectral range of pressure indicators, facilitating remote pressure readouts. In this work, the system of Nd^{3+} and Cr^{3+} in $La_3Ga_5GeO_{14}$ was used as a model example.

EXPERIMENTAL SECTION

$La_3Ga_5GeO_{14}$ powders doped with different concentrations of Nd^{3+} and Cr^{3+} ions were synthesized by a solid-state reaction. For this purpose, stoichiometric amounts of lanthanum oxide (La_2O_3 of 99.99% purity from Stanford Materials Corporation), gallium(III) nitrate hydrate ($Ga(NO_3)_3{\cdot}xH_2O$ of 99.999% purity from Alfa Aesar), germanium oxide (GeO_2 of 99.999% purity), neodymium oxide (Nd_2O_3 of 99.99% purity from Alfa Aesar), and chromium(III) nitrate nonahydrate ($Cr(NO_3)_3{\cdot}9H_2O$ of 99.99% purity from Alfa Aesar) were ground under hexane in an agate mortar and then transferred to an alumina crucible and annealed in a furnace at 1300 °C for 10 h in an air atmosphere.

The obtained materials were then examined by X-ray powder diffraction (XRD) using a PANalytical X'Pert Pro diffractometer in Bragg−Brentano geometry equipped with an Anton Paar TCU1000 N temperature-control unit using Ni-filtered Cu Kα radiation (V = 40 kV, I = 30 mA). Measurements were made in the range of 10−90°, and the measurement time is ∼1 h. Excitation spectra were measured on a FLS1000 spectrometer from Edinburgh Instruments. The excitation source was a 450 W xenon lamp, and the R5509-72 photomultiplier tube in a nitrogen flow-cooled housing from Hamamatsu was used as a detector. The temperature-dependent emission spectra were measured using the same system with a 445 nm laser diode from CNI Lasers used as the excitation source and a THMS 600 heating−cooling stage from Linkam to control the temperature with a precision of 0.1 K. Luminescence spectra as a function of pressure were measured with 445 nm (LGG Cr^{3+} and LGG Cr^{3+}, Nd^{3+}) and 532 nm (LGG Nd^{3+}) laser diode excitation. Pressure was applied to the sample thanks to a gas membrane that transmitted it to the Diacell μScopeDAC-RT(G) diamond anvil cell (DAC) with 0.4 mm diamond culets. The gas used in the system is compressed nitrogen, which was supplied to the membrane using a Druck PACE 5000, which allowed for a relatively controlled change in pressure. An accurate change of the parameter under study was possible by controlling the spectral shift of the R_1 ruby line. The sample was placed in a ∼140 μm hole drilled in a 250 μm thick stainless steel gasket. The pressure transmission medium was a methanol−ethanol solution (4/1). A custom Matlab (Mathworks R2019b) routine was prepared to divide the two images, aiming to obtain a ratiometric image and plot cross sections of the ratio.

https://doi.org/10.1021/acsaom.2c00198
ACS Appl. Opt. Mater. XXXX, XXX, XXX−XXX

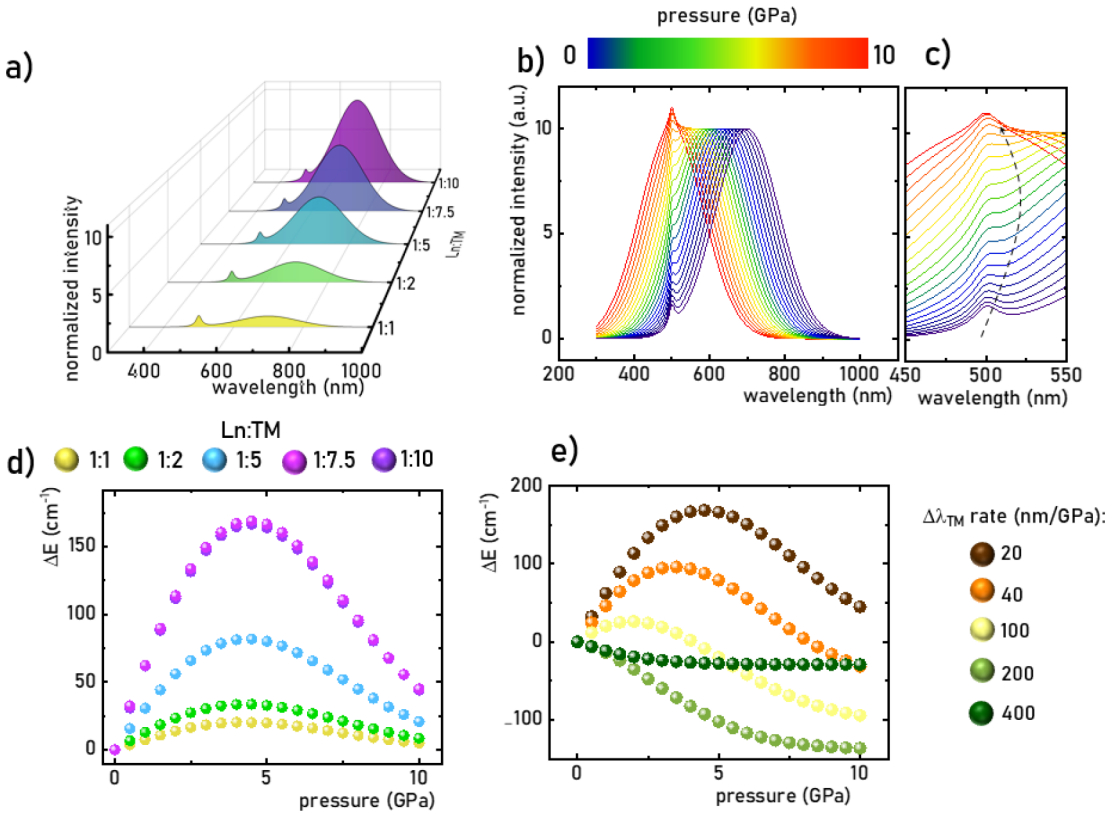

Figure 2. (a) Simulated emission band for different intensity ratios of lanthanide (simulated by Lorentz profile) and TM ions (simulated by a Gaussian band) emission. (b) Calculated emission spectra shape for Ln/TM = 1:7.5 as a function of pressure. (c) Zoomed-in image of the spectral range of the Lorentz band. (d) ΔE as a function of pressure for different Ln/TM ratios. (e) ΔE as a function of the spectral shift rate (for Ln/TM = 1:7.5).

RESULTS AND DISCUSSION

Simulations

The main hypothesis presented in the Introduction about the possibility of sensitizing Ln^{3+} emissions to pressure changes by codoping the host material with TM ions was verified by numerical calculations (Figure 2). For this purpose, a system composed of two emission bands was used, namely, the Lorentz curve representing the 4f−4f spectral line of Ln^{3+} ions and the Gauss curve representing the d−d emission band of TM ions. In the performed calculations, the position of the Ln^{3+} emission band was assumed to be independent of pressure, and the rate of the spectral shift of the TM band as a function of pressure was modulated. The augmented spectral shift of the Ln^{3+} band is due to the overlap between the two signals analyzed. Therefore, the ratio of the intensities of the Ln^{3+} and TM bands should significantly affect this effect. The calculations carried out with a constant rate of the spectral shift of the TM band and a variable ratio of the intensities of the Ln^{3+} and TM bands (Ln/TM) (Figure 2a) revealed that, as the Ln/TM ratio decreases, the obtained shift of the Ln^{3+} band maximum increases to a certain value, after which it decreases again (Figure 2b and c). The change in the monotonicity of the band shift is related to the fact that, when the TM band approaches the maximum of the Ln^{3+}emission, a shift toward shorter wavelengths is observed. By analyzing the dependence of the change in energy of the barycenter of the Ln^{3+} band (ΔE), it can be seen that the largest changes are observed when Ln/TM is 1:7.5, and a slight decrease in the maximum achieved value of ΔE is observed for lower values of Ln/TM ratio. A larger change in ΔE results in a higher absolute sensitivity of a luminescence manometer. Therefore, this intensity ratio of the two signals was preserved in further calculations. This analysis clearly reveals that, in order to achieve high sensitivity of the luminescent manometer in the presented approach, it is important to maintain a relatively low emission signal of the Ln^{3+} band with respect to TM. This can be achieved by optimizing the relative concentration of the Ln^{3+} ions to TM. However, it should also be noted that a low intensity of Ln^{3+} can hinder the readout of the maximum of its emission band and thus, through an increasing noise-to-signal ratio, reduce the precision of the readout. Preserving the Ln/TM = 1:7.5 ratio, the effect of the rate of the pressure-induced shift of the TM band was analyzed (Figure 2d). Note, the efficiency of this effect depends on the initial spectral distance between the Ln and TM emission bands at ambient pressure; hence, it should always be taken into account (300 nm in this case). As can be clearly seen, for a low spectral shift rate the highest changes are observed, and an increase in the shift rate of the TM band causes a decrease in the maximum ΔE value, until the sign of ΔE becomes the reverse, which represents a shift of the Ln^{3+} band toward shorter wavelengths (Figure 2e). When the rate of change approaches the initial spectral difference between the Ln^{3+} and TM bands at ambient pressure, the ΔE is close to 0.

Experimental Implementation

The structure of the $La_3Ga_5GeO_{14}$ crystal belongs to the trigonal system with space group $P321$ (150). The material is characterized by the $A_3BC_3D_2O_{14}$-type structure, where in the

https://doi.org/10.1021/acsaom.2c00198
ACS Appl. Opt. Mater. XXXX, XXX, XXX−XXX

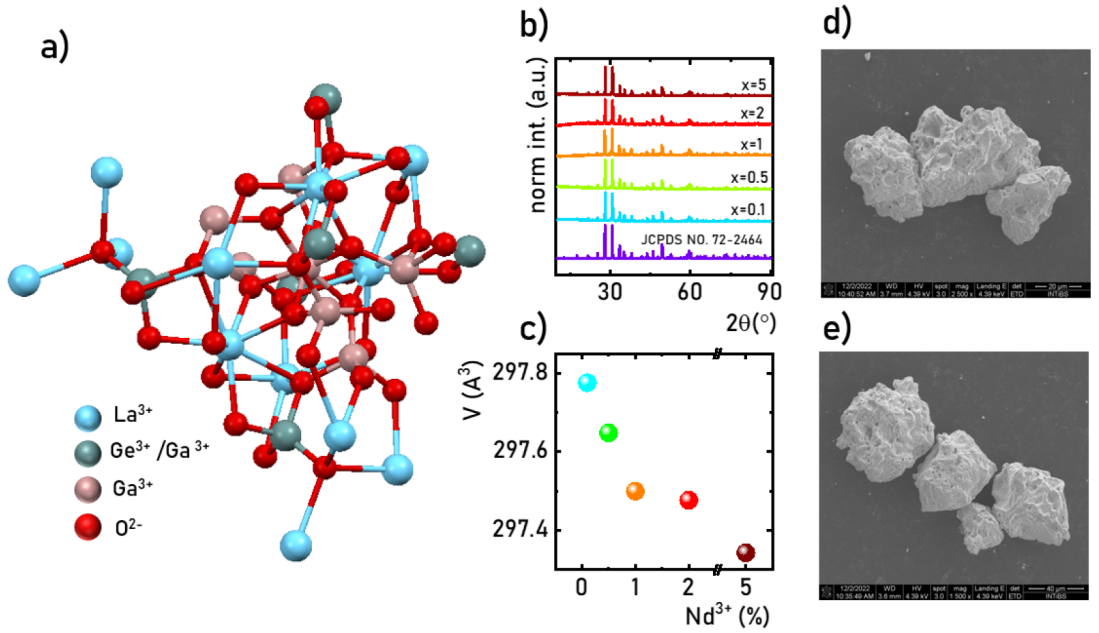

Figure 3. (a) Visualization of the crystal structure of $La_3Ga_5GeO_{14}$. (b) XRD patterns of $La_3Ga_5GeO_{14}$:0.5% Cr^{3+},Nd^{3+} for different concentrations of Nd^{3+} ions. (c) Calculated cell unit volume as a function of Nd^{3+} concentration. (d) Representative SEM images of $La_3Ga_5GeO_{14}$:0.5%Nd^{3+} and (e) $La_3Ga_5GeO_{14}$:0.5%Nd^{3+},Cr^{3+}.

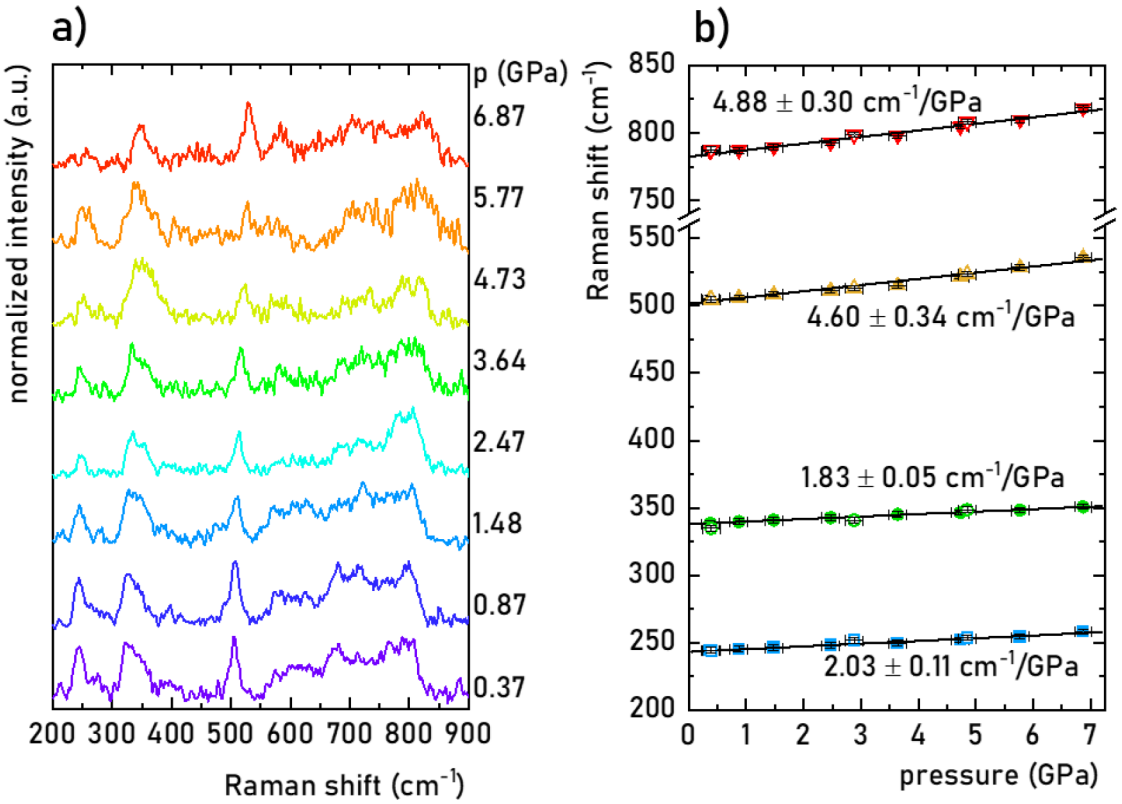

Figure 4. (a) Normalized Raman spectra for the $La_3Ga_5GeO_{14}$ material measured for different pressure values during the compression cycle. (b) Determined energies (peak centroids) of the most intense phonon modes as a function of pressure. Filled symbols represent compression data, and empty ones represent decompression data. The continuous lines are the linear fits applied for determination of the pressure shift rates of the corresponding Raman modes.

case of $La_3Ga_5GeO_{14}$ the A cationic sites are occupied by La^{3+} and the B cationic sites are occupied by Ga^{3+} surrounded by eight and six oxygen anions forming a dodecahedron and an octahedron, respectively.[31−35] Sites C and D are both surrounded by four oxygen anions forming a tetrahedron. The C site is occupied by Ga^{3+}, whereas the D site is partially occupied by Ge^{4+} and Ga^{3+} (Figure 2a). Due to the same charge and similarity of ionic radii (r_{Cr3+} = 0.615 Å; $r_{Ga(VIII)3+}$ =

https://doi.org/10.1021/acsaom.2c00198
ACS Appl. Opt. Mater. XXXX, XXX, XXX−XXX

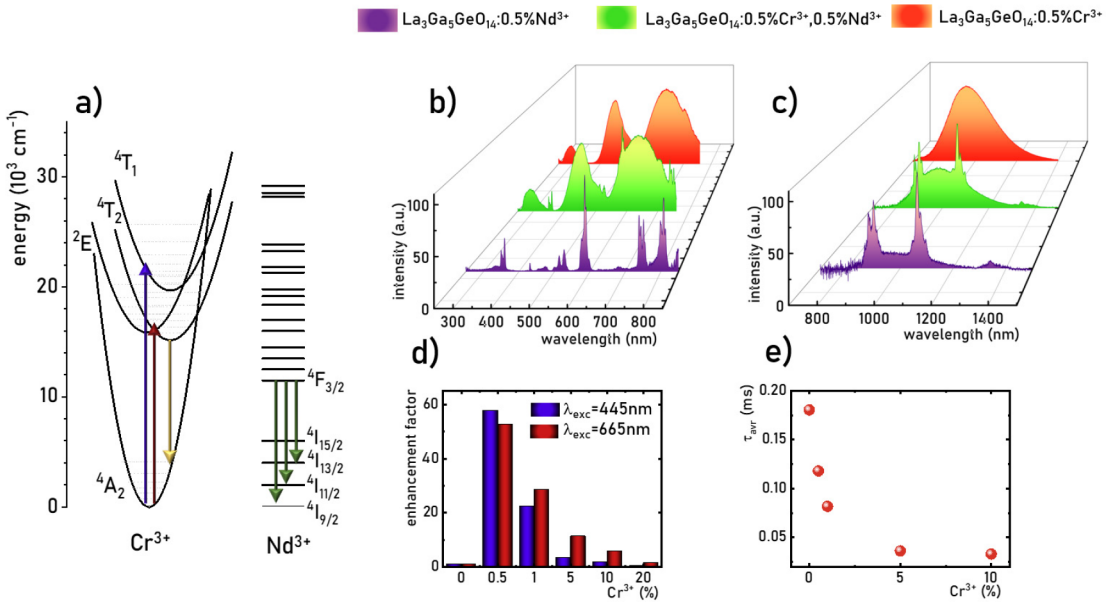

Figure 5. (a) Simplified energy level diagram of Nd^{3+} ions and configurational coordination energy diagram of Cr^{3+} ions in a weak crystal field. Comparison of (b) excitation and (c) emission spectra measured at 123 K for the $La_3Ga_5GeO_{14}$:Nd^{3+}, $La_3Ga_5GeO_{14}$:Nd^{3+},Cr^{3+}, and $La_3Ga_5GeO_{14}$:Cr^{3+} materials. (d) Influence of the Cr^{3+} concentration on the integrated emission intensity of the $^4F_{3/2} \rightarrow {}^4I_{11/2}$ emission band of Nd^{3+} upon λ_{exc} = 445 nm and λ_{exc} = 665 nm. (e) τ_{avr} values of the $^4F_{3/2}$ state of Nd^{3+} measured at 123 K as a function of Cr^{3+} concentration.

0.62 Å), the Cr^{3+} ions most plausibly replace the Ga^{3+} ions in the crystal lattice. On the other hand, the Nd^{3+} ions, which have an ionic radius of r_{Nd3+} = 1.109 Å in the dodecahedral configuration, substitute the La^{3+} ions with r_{La3+} = 1.16 Å. A relatively large Ga^{3+}−O^{2-} distance in this structure results in a weak crystal field strength affecting the Cr^{3+} ions. The comparative analysis of the diffraction patterns of the samples doped with 0.5% of Cr^{3+} and different concentrations of Nd^{3+} (Figure 3b) with the standard $La_3Ga_5GeO_{14}$ (JSPDS no. 72-2646) reveals that the introduction of dopant ions does not affect the phase purity of the powders. The increase in the Nd^{3+} concentration results in the gradual shift of the diffraction reflections toward higher 2Θ angles, which indicates the reduction of the cell unit. This is expected due to the difference in the ionic radii of Nd^{3+} and La^{3+} ions. The performed Rietveld refinement calculations confirm this effect, revealing that the size of the unit cell volume (V) shrinks from 297.79 $Å^3$ for the $La_3Ga_5GeO_{14}$:0.5%Cr^{3+} to 297.36 $Å^3$ for the $La_3Ga_5GeO_{14}$:0.5%Cr^{3+},5%Nd^{3+} (Figure 3c). As shown in the analysis of the scanning electron microscopy (SEM) images, the synthesized powders consist of microparticles of ∼40 μm in diameter (Figure 3d and e).

We investigated the structural stability of the investigated material with pressure by measuring the Raman spectra for the host matrix (undoped material), to avoid luminescence from the optically active ions that typically obscure and superimpose with Raman bands. The recorded Raman spectra for the $La_3Ga_5GeO_{14}$ sample at ambient pressure show few broad bands, where the most intense ones are located at approximately 240, 340, 500, and 780 cm^{-1} (at ambient conditions), as presented in Figure 4a. As pressure increases, i.e., compressing the compound studied, the energies of the phonon modes increase, so the corresponding Raman bands shift toward higher wavenumbers, which can be clearly seen in Figure 4b. This phenomenon is associated with bonds shortening, namely, a decrease of the distances between the atoms, in the compressed materials. The observed spectral shifts are monotonous and linear, confirming good structural stability of the examined material and the absence of phase transitions in the investigated pressure range. The determined shift rates for the corresponding Raman bands are listed in Table S1. It is worth noting that the observed deterioration of the Raman signal with pressure, i.e., decreasing the signal-to-noise ratio, is due to the increasing strains and crystal defects in the compressed structure, as commonly observed for such kinds of measurements. Upon pressure release (decompression process), the shape and spectral positions of all Raman peaks come back to the initial state, as shown in Figure 4b and Figure S1 (spectra recorded during the decompression run). The good agreement between the compression and decompression data confirm the reversibility of the process (which is critical for pressure-sensing purposes) and indicate the possibility of application of the synthesized $La_3Ga_5GeO_{14}$ material as an optical manometer.

The description of emission generation in the $La_3Ga_5GeO_{14}$:Cr^{3+},Nd^{3+} system is facilitated by the analysis of the energy diagram of Nd^{3+} levels and the configurational coordinate diagram of Cr^{3+}. In the case of $La_3Ga_5GeO_{14}$, a weak crystal field affects the Cr^{3+} ions. Hence, the parabola of the $^4T_2$ level is below the ^2E one. Therefore, the excitation beam allows electron transfer from the $^4A_2$ ground level to the $^4T_2$ or $^4T_1$ states followed by nonradiative transitions that lead to the population of the emitting $^4T_2$ state. Radiative depopulation of this level results in the occurrence of a broad emission band with a maximum at ∼990 nm. On the other hand, in the case of the Nd^{3+} ions, a relatively dense energy level diagram shows that upon an optical excitation the electron transferred from the $^4I_{9/2}$ ground state to the excited levels after the optical excitation undergoes efficient nonradiative processes, resulting in the population of the $^4F_{3/2}$ metastable state. The depopulation of this state leads to the formation of three emission bands at about 890, 1060, and 1350 nm, which correspond to the $^4F_{3/2} \rightarrow {}^4I_{9/2}$, $^4F_{3/2} \rightarrow {}^4I_{11/2}$, and $^4F_{3/2} \rightarrow {}^4I_{13/2}$ electron transitions, respectively. As

https://doi.org/10.1021/acsaom.2c00198
ACS Appl. Opt. Mater. XXXX, XXX, XXX−XXX

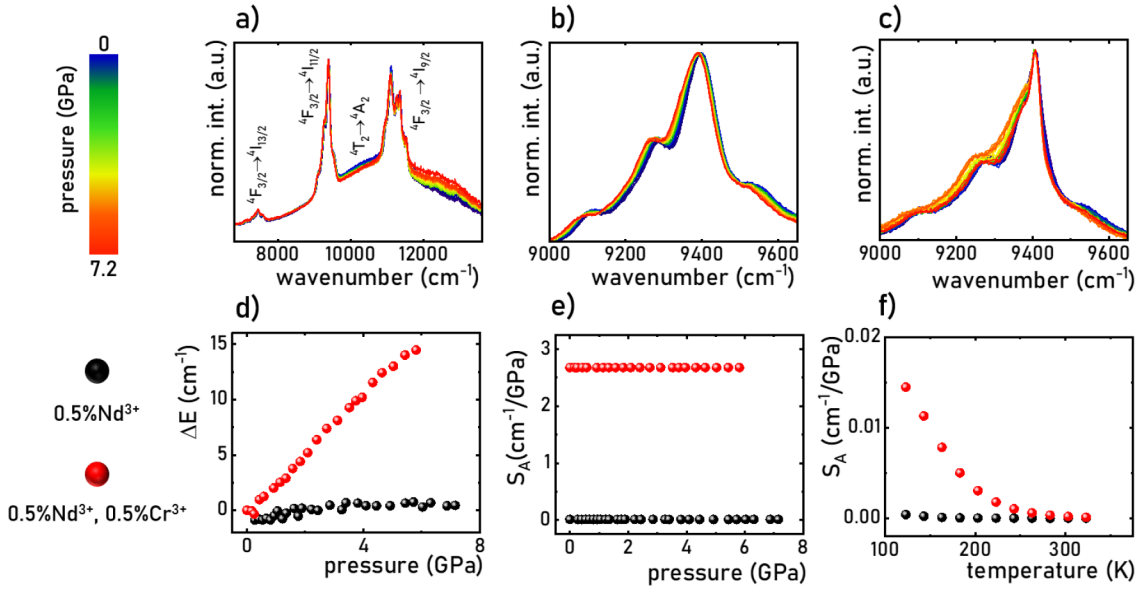

Figure 6. (a) Emission spectra of $La_3Ga_5GeO_{14}$:0.5%Nd^{3+},0.5%Cr^{3+} measured as a function of pressure. Comparison of the emission spectra of (b) $La_3Ga_5GeO_{14}$:0.5%Nd^{3+},0.5%Cr^{3+} and (c) $La_3Ga_5GeO_{14}$:0.5%Nd^{3+} limited to the spectral range of the $^4F_{3/2} \rightarrow {}^4I_{11/2}$ emission band of Nd^{3+} ions. (d) ΔE as a function of pressure for Nd^{3+} and Cr^{3+},Nd^{3+} doped phosphors and the (e) corresponding S_A values. (f) S_A values measured as a function of temperature.

indicated by the analysis of the $La_3Ga_5GeO_{14}$:Cr^{3+} excitation spectra, $^4T_2 \rightarrow {}^4A_2$ emission can be obtained by excitation into one of the spectrally broad $^4A_2 \rightarrow {}^4T_1$ and $^4A_2 \rightarrow {}^4T_2$ bands, with maxima at about 450 and 650 nm, respectively (Figure 5b; see also Figure S2 for emission spectra of $La_3Ga_5GeO_{14}$:Cr^{3+} at different concentrations of Cr^{3+} ions). In the excitation spectra of the $La_3Ga_5GeO_{14}$:Nd^{3+}, a number of spectrally narrow absorption lines characteristic of 4f−4f transitions can be observed. Importantly, many of these bands spectrally overlap with the broad absorption bands of Cr^{3+} ions, which enables efficient $Cr^{3+} \rightarrow Nd^{3+}$ energy transfer (Figure S4). This energy transfer is confirmed by the fact that, when measuring the excitation spectrum of Nd^{3+} ions (λ_{em} = 1060 nm) for the $La_3Ga_5GeO_{14}$:Cr^{3+},Nd^{3+} material, both spectrally narrow 4f−4f bands of Nd^{3+} and broad bands of Cr^{3+} ions are observed (Figure 5b and Figure S5). An optical excitation of the $La_3Ga_5GeO_{14}$:Cr^{3+},Nd^{3+} sample at λ_{exc} = 445 nm results in an emission spectrum consisting of both Nd^{3+} bands, as well as a broad $^4T_2 \rightarrow {}^4A_2$ band of Cr^{3+} ions. Importantly, the $^4T_2 \rightarrow {}^4A_2$ band spectrally overlaps with all Nd^{3+} bands. The observed energy transfer between Cr^{3+} ions and Nd^{3+} ions is particularly important because, due to the much higher absorption cross section of Cr^{3+} ions compared to the Nd^{3+} counterpart, its occurrence leads to the enhancement of the luminescence brightness of Nd^{3+} ions, which is particularly important from an application perspective. As demonstrated by comparative characterization using an excitation beam λ_{exc} = 445 nm, a nearly 60-fold more intense luminescence of Nd^{3+} ions was observed for the sample codoped with 0.5Nd^{3+},0.5%Cr^{3+} compared to its solely Nd^{3+}-doped counterpart (Figure S6). Further increases in the concentration of Cr^{3+} ions gradually reduced this enhancement. Nevertheless, in each of the analyzed cases of codoped samples, the luminescence intensity of Nd^{3+} ions significantly exceeded that of the sample doped only with Nd^{3+} ions. An equally pronounced though less spectacular effect was observed using an λ_{exc} = 668 nm excitation beam. The decrease in the observed enhancement may originate from an increase in the probability of $Nd^{3+} \rightarrow Cr^{3+}$ back-energy transfer. Confirmation of this conjecture can be provided by the analysis of luminescence decay times of Nd^{3+} from the $^4F_{3/2}$ level. The lifetime (τ) of the $^4F_{3/2}$ level for the $La_3Ga_5GeO_{14}$:0.5%Nd^{3+} sample is equal to ∼180 μs. As the concentration of Cr^{3+} ions increases, the τ gradually shortens down to 30 μs for the $La_3Ga_5GeO_{14}$:0.5%Nd^{3+},10%Cr^{3+} sample. This shortening is related to $Nd^{3+} \rightarrow Cr^{3+}$ energy transfer, whose probability increases as the average distance between Nd^{3+} and Cr^{3+} ions shortens, as happens when the concentration of Cr^{3+} in the sample increases.

To experimentally verify the proposed hypothesis, the emission spectra of the $La_3Ga_5GeO_{14}$:Cr^{3+},Nd^{3+} material were measured as a function of pressure in the 0−7 GPa pressure range. Analogously as in the case of the $La_3Ga_5GeO_{14}$:Cr^{3+} compound, a spectral shift of the $^4T_2 \rightarrow {}^4A_2$ band toward higher energies (shorter wavelengths) is observed with increasing pressure (Figure S7). This effect is related to an increase in the crystal field strength affecting the Cr^{3+} ions, which originally results from the pressure-induced shortening of the average Cr^{3+}−O^{2-} distance. By superimposing this effect with the narrow-band emission of Nd^{3+} ions, an increase in pressure causes an apparent spectral shift in the bands of Nd^{3+} ions (Figure 6a). Due to the highest intensity of the $^4F_{3/2} \rightarrow {}^4I_{11/2}$ band, further considerations will be focused on this band only. As can be clearly seen, Cr^{3+} doping sensitizes the emission of Nd^{3+} to pressure changes, i.e., compression of the material (Figure 6b). This can be understood by comparing the obtained results with the spectra of the $La_3Ga_5GeO_{14}$:Nd^{3+}-doped only with Nd^{3+} ions (Figure 6c). The analysis shows a monotonic, linear change in the energy of the $^4F_{3/2} \rightarrow {}^4I_{11/2}$ band over the entire range of the analyzed pressure values. The total shift of the band maximum is ΔE = 15 cm^{-1}, while the same band for the $La_3Ga_5GeO_{14}$:Nd^{3+} sample does not undergo any spectral displacement (Figure 6d). It should be emphasized that the

https://doi.org/10.1021/acsaom.2c00198
ACS Appl. Opt. Mater. XXXX, XXX, XXX−XXX

ΔE decreases monotonically with the pressure release (during decompression process), which confirms that the applied pressure does not permanently affect the structure of the $La_3Ga_5GeO_{14}$, and the observed changes are reversible. The observed spectral shift can be quantified by calculating the absolute pressure sensitivity (S_A),

$$S_A = \frac{\Delta E}{\Delta p} \quad (1)$$

where ΔE represents the change of the energy of the band centroid corresponding to the change of the pressure by Δp. In the case of $La_3Ga_5GeO_{14}:Nd^{3+}$, the undetected spectral band shift with increasing pressure results in $S_A = 0$. On the other hand, the linear change in ΔE as a function of pressure observed for $La_3Ga_5GeO_{14}$:0.5%Nd^{3+},0.5%Cr^{3+} results in a constant shift rate of the band centroid over the entire analyzed pressure range, resulting in $S_A = 2.8 \pm 0.002$ cm^{-1}/GPa. From a manometric perspective, it is important that the pressure readouts are barely or completely independent of changes of other physical parameters, especially temperature. Therefore, the spectral shift of the $^4F_{3/2} \rightarrow {}^4I_{11/2}$ band was analyzed over a wide temperature range of 77−330 K in ambient pressure (Figures S8 and S9). The analysis showed that in the low-temperature range (<200 K) only a little variation is observed, manifesting in nonzero values of $S_A(T)$. However, the temperature drift is negligibly small, decreasing from 0.015 ± 0.002 cm^{-1}/K to close to 0 above 250 K. At higher temperature values, no variability in the position of this band is observed. As shown, the codoping with Cr^{3+} ions leads to the sensibilization of the Nd^{3+} emission to pressure changes, and such designed luminescent manometers can be an interesting alternative to Cr^{3+}-based pressure gauges, like ruby, whose emission line is highly temperature-dependent. Although the presented results are very optimistic, as shown in Figure 2 the further optimization of the Ln/TM ratio and the rate of the pressure-induced shift of TM will lead to a more spectacular augment of the spectral shift of Ln^{3+} and to the development of more sensitive luminescent manometers in the future.

CONCLUSIONS

In the present work, a new strategy to enhancement of the pressure-induced spectral shift of the emission band of Ln^{3+} ions by codoping the systems with Ln^{3+} and TM ions is proposed. As shown by simulations, the high sensitivity of the broad emission band of TM to pressure changes and the spectral overlap between the Ln^{3+} and TM bands results in the spectral shift of the 4f−4f emission band of Ln^{3+} ions. The proposed approach was experimentally verified on a $La_3Ga_5GeO_{14}:Nd^{3+},Cr^{3+}$ system codoped with Cr^{3+} and Nd^{3+}. As shown through the spectral overlap between the $^4T_2 \rightarrow {}^4A_2$ band of Cr^{3+} ions with the $^4F_{3/2} \rightarrow {}^4I_{11/2}$ band of Nd^{3+}, the pressure-independent $^4F_{3/2} \rightarrow {}^4I_{11/2}$ line in $La_3Ga_5GeO_{14}:Nd^{3+}$ starts to shift monotonically as a function of applied pressure with an absolute sensitivity of $S_A = 2.8$ cm^{-1}/GPa in $La_3Ga_5GeO_{14}:Nd^{3+},Cr^{3+}$. Due to its versatility, the presented approach will allow the development of new luminescent manometers with a high-precision pressure readout that emit in any spectral range dependent on the selection of Ln^{3+} ions.

ASSOCIATED CONTENT

Supporting Information

The Supporting Information is available free of charge at https://pubs.acs.org/doi/10.1021/acsaom.2c00198.

Raman spectra of $La_3Ga_5GeO_{14}$ measured at different pressures; emission spectra of $La_3Ga_5GeO_{14}:Nd^{3+},Cr^{3+}$ measured as a function of temperature and pressure; and excitation spectra of $La_3Ga_5GeO_{14}:Nd^{3+},Cr^{3+}$ (PDF)

AUTHOR INFORMATION

Corresponding Author

L. Marciniak − *Institute of Low Temperature and Structure Research, Polish Academy of Sciences, 50-422 Wrocław, Poland;* orcid.org/0000-0001-5181-5865; Email: l.marciniak@intibs.pl

Authors

M. Pieprz − *Institute of Low Temperature and Structure Research, Polish Academy of Sciences, 50-422 Wrocław, Poland*

M. Runowski − *Faculty of Chemistry, Adam Mickiewicz University, 61-614 Poznan, Poland; Departamento de Física, IUdEA and MALTA-Consolider Team, Universidad de La Laguna, E-38200 San Cristóbal de La Laguna, Santa Cruz de Tenerife, Spain*

K. Ledwa − *Institute of Low Temperature and Structure Research, Polish Academy of Sciences, 50-422 Wrocław, Poland;* orcid.org/0000-0003-2826-7623

J. J. Carvajal − *Departament Química Física i Inorgànica, Universitat Rovira i Virgili, E-43007 Tarragona, Spain;* orcid.org/0000-0002-4389-7298

A. Bednarkiewicz − *Institute of Low Temperature and Structure Research, Polish Academy of Sciences, 50-422 Wrocław, Poland;* orcid.org/0000-0003-4113-0365

Complete contact information is available at: https://pubs.acs.org/10.1021/acsaom.2c00198

Notes

The authors declare no competing financial interest.

ACKNOWLEDGMENTS

This work was supported by the National Science Center (NCN) Poland under Project no. DEC-UMO-2020/37/B/ST5/00164. M.R. acknowledges support from Fondo Social Europeo and Agencia Estatal de Investigación (RYC2020-028778-I/AEI/10.13039/501100011033).

REFERENCES

(1) Goderski, S.; Runowski, M.; Woźny, P.; Lavín, V.; Lis, S. Lanthanide Upconverted Luminescence for Simultaneous Contactless Optical Thermometry and Manometry-Sensing under Extreme Conditions of Pressure and Temperature. *ACS Appl. Mater. Interfaces* **2020**, *12* (36), 40475−40485.

(2) Zheng, T.; Luo, L.; Du, P.; Lis, S.; Rodríguez-Mendoza, U. R.; Lavín, V.; Martín, I. R.; Runowski, M. Pressure-Triggered Enormous Redshift and Enhanced Emission in $Ca_2Gd_8Si_6O_{26}:Ce^{3+}$ Phosphors: Ultrasensitive, Thermally-Stable and Ultrafast Response Pressure Monitoring. *Chem. Eng. J.* **2022**, *443*, 136414.

(3) Szymczak, M.; Woźny, P.; Runowski, M.; Pieprz, M.; Lavín, V.; Marciniak, L. Temperature Invariant Ratiometric Luminescence Manometer Based on Cr^{3+} Ions Emission. *Chem. Eng. J.* **2023**, *453*, 139632.

(4) Lange, V.; Lima, F.; Kühlke, D. Multicolour LED in Luminescence Sensing Application. *Sensors Actuators, A Phys.* **2011**, *169* (1), 43−48.
(5) Shi, P.; Duan, Y.; Wei, W.; Xu, Z.; Li, Z.; Han, T. A Turn-on Type Mechanochromic Fluorescent Material Based on Defect-Induced Emission: Implication for Pressure Sensing and Mechanical Printing. *J. Mater. Chem. C* **2018**, *6* (10), 2476−2482.
(6) Lv, S.; Shanmugavelu, B.; Wang, Y.; Mao, Q.; Zhao, Y.; Yu, Y.; Hao, J.; Zhang, Q.; Qiu, J.; Zhou, S. Transition Metal Doped Smart Glass with Pressure and Temperature Sensitive Luminescence. *Adv. Opt. Mater.* **2018**, *6* (21), 1800881.
(7) Antoniak, M. A.; Zelewski, S. J.; Oliva, R.; Żak, A.; Kudrawiec, R.; Nyk, M. Combined Temperature and Pressure Sensing Using Luminescent $NaBiF_4$:Yb,Er Nanoparticles. *ACS Appl. Nano Mater.* **2020**, *3* (5), 4209−4217.
(8) Petit, R. R.; Michels, S. E.; Feng, A.; Smet, P. F. Adding Memory to Pressure-Sensitive Phosphors. *Light Sci. Appl.* **2019**, *8* (1), 124.
(9) Otto, S.; Harris, J. P.; Heinze, K.; Reber, C. Molecular Ruby under Pressure. *Angew. Chemie - Int. Ed.* **2018**, *57* (34), 11069−11073.
(10) Lorenzon, M.; Pinchetti, V.; Bruni, F.; Bae, W. K.; Meinardi, F.; Klimov, V. I.; Brovelli, S. Single-Particle Ratiometric Pressure Sensing Based on "Double-Sensor" Colloidal Nanocrystals. *Nano Lett.* **2017**, *17* (2), 1071−1081.
(11) Zhang, M.; Zhao, L.; Zhao, R.; Li, Z.; Liu, Y.; Duan, Y.; Han, T. A Mechanochromic Luminescent Material with Aggregation-Induced Emission: Application for Pressure Sensing and Mapping. *Spectrochim. Acta - Part A Mol. Biomol. Spectrosc.* **2019**, *220*, 117125.
(12) Zhang, D.; Zheng, B.; Zheng, Z.; Li, L.; Yang, Q.; Song, Y.; Zou, B.; Zou, H. Multifunctional $Ca_9NaZn_{1-Y}Mg_y(PO_4)_7$:$Eu^{2+}$ Phosphor for Full-Spectrum Lighting, Optical Thermometry and Pressure Sensor Applications. *Chem. Eng. J.* **2022**, *431*, 133805.
(13) Szymczak, M.; Runowski, M.; Lavín, V.; M, L. Highly Pressure-Sensitive, Temperature Independent Luminescence Ratiometric Manometer Based on MgO:Cr^{3+} Nanoparticles. *Laser Photonics Rev.* **2023**, 2200801.
(14) Kim, Y.; Roy, S.; Jung, G. Y.; Oh, J. S.; Kim, G. W. Dual Optical Signal-Based Intraocular Pressure-Sensing Principle Using Pressure-Sensitive Mechanoluminescent ZnS:Cu/PDMS Soft Composite. *Sci. Rep.* **2019**, *9* (1), 15215.
(15) Peng, D.; Zhong, Z.; Cai, T.; Guo, S.; Zhao, X.; Liu, Y. Integration of Pressure-Sensitive Paint with Persistent Phosphor: A Light-Charged Pressure-Sensing System. *Rev. Sci. Instrum.* **2018**, *89* (8), 085003.
(16) Zheng, T.; Sójka, M.; Woźny, P.; Martín, I. R.; Lavín, V.; Zych, E.; Lis, S.; Du, P.; Luo, L.; Runowski, M. Supersensitive Ratiometric Thermometry and Manometry Based on Dual-Emitting Centers in Eu^{2+}/Sm^{2+}-Doped Strontium Tetraborate Phosphors. *Adv. Opt. Mater.* **2022**, *10* (20), 2201055.
(17) Zhou, P.; Zhang, Q.; Peng, F.; Sun, B.; Dou, X.; Liu, B.; Han, D.; Xue, Y.; Ding, K. Optical Properties of Nd^{3+} Ions Doped $GdTaO_4$ for Pressure and Temperature Sensing. *J. Rare Earths* **2022**, *40* (6), 870−877.
(18) Rodríguez-Mendoza, U. R.; León-Luis, S. F.; Muñoz-Santiuste, J. E.; Jaque, D.; Lavín, V. Nd^{3+}-Doped $Ca_3Ga_2Ge_3O_{12}$ Garnet: A New Optical Pressure Sensor. *J. Appl. Phys.* **2013**, *113* (21), 213517.
(19) Wisser, M. D.; Chea, M.; Lin, Y.; Wu, D. M.; Mao, W. L.; Salleo, A.; Dionne, J. A. Strain-Induced Modification of Optical Selection Rules in Lanthanide-Based Upconverting Nanoparticles. *Nano Lett.* **2015**, *15* (3), 1891−1897.
(20) Barnett, J. D.; Block, S.; Piermarini, G. J. An Optical Fluorescence System for Quantitative Pressure Measurement in the Diamond-Anvil Cell. *Rev. Sci. Instrum.* **1973**, *44* (1), 1−9.
(21) Novita, M.; Marlina, D.; Cholifah, N.; Ogasawara, K. Study on the Molecular Orbital Energies of Ruby under Pressure. *Opt. Mater. (Amst).* **2020**, *109*, 110375.
(22) Schuster, B.; Weikusat, C.; Miletich, R.; Trautmann, C.; Neumann, R.; Fujara, F. Influence of Radiation Damage on Ruby as a Pressure Gauge. *Phys. Rev. B - Condens. Matter Mater. Phys.* **2010**, *82* (18), 184110.
(23) Wen-Chen, Z. Explanation of the Pressure-Induced Red Shifts of ^2E-$^4A_2$ Transition Line for Cr^{3+} Ions in the Two Sites of Chrysoberyl. *Solid State Commun.* **1996**, *98* (2), 167−169.
(24) Dong, H.; Dorfman, S. M.; Wang, J.; He, D.; Duffy, T. S. The Strength of Ruby from X-Ray Diffraction under Non-Hydrostatic Compression to 68 GPa. *Phys. Chem. Miner.* **2014**, *41* (7), 527−535.
(25) Runowski, M.; Woźny, P.; Stopikowska, N.; Guo, Q.; Lis, S. Optical Pressure Sensor Based on the Emission and Excitation Band Width (Fwhm) and Luminescence Shift of Ce^{3+}-Doped Fluorapatite - High-Pressure Sensing. *ACS Appl. Mater. Interfaces* **2019**, *11* (4), 4131−4138.
(26) Barzowska, J.; Lesniewski, T.; Mahlik, S.; Seo, H. J.; Grinberg, M. $KMgF_3$:Eu^{2+} as a New Fluorescence-Based Pressure Sensor for Diamond Anvil Cell Experiments. *Opt. Mater. (Amst).* **2018**, *84*, 99−102.
(27) Wang, Y.; Seto, T.; Ishigaki, K.; Uwatoko, Y.; Xiao, G.; Zou, B.; Li, G.; Tang, Z.; Li, Z.; Wang, Y. Pressure-Driven Eu^{2+}-Doped $BaLi_2Al_2Si_2N_6$: A New Color Tunable Narrow-Band Emission Phosphor for Spectroscopy and Pressure Sensor Applications. *Adv. Funct. Mater.* **2020**, *30* (34), 2001384.
(28) Zheng, T.; Sójka, M.; Runowski, M.; Woźny, P.; Lis, S.; Zych, E. Tm^{2+} Activated SrB_4O_7 Bifunctional Sensor of Temperature and Pressure—Highly Sensitive, Multi-Parameter Luminescence Thermometry and Manometry. *Adv. Opt. Mater.* **2021**, *9* (22), 2101507.
(29) Jovanić, B. R.; Andreeta, J. P. $GdAlO_3$:Cr^{3+} as a New Pressure Sensor. *Phys. Scr.* **1999**, *59* (4), 274−276.
(30) Back, M.; Ueda, J.; Hua, H.; Tanabe, S. Predicting the Optical Pressure Sensitivity of $^2E \rightarrow {}^4A_2$ Spin-Flip Transition in Cr^{3+}-Doped Crystals. *Chem. Mater.* **2021**, *33* (9), 3379−3385.
(31) Lu, J.; Mu, Z.; Zhu, D.; Wang, Q.; Wu, F. Luminescence Properties of Eu^{3+} Doped $La_3Ga_5GeO_{14}$ and Effect of Bi^{3+} Co-Doping. *J. Lumin.* **2018**, *196*, 50−56.
(32) Yan, W.; Liu, F.; Lu, Y.-Y.; Wang, X.-J.; Yin, M.; Pan, Z. Near Infrared Long-Persistent Phosphorescence in $La_3Ga_5GeO_{14}$:Cr^{3+} Phosphor. *Opt. Express* **2010**, *18* (19), 20215.
(33) Wu, Y.; Li, Y.; Qin, X.; Chen, R.; Wu, D.; Liu, S.; Qiu, J. Dual Mode NIR Long Persistent Phosphorescence and NIR-to-NIR Stokes Luminescence in $La_3Ga_5GeO_{14}$: Cr^{3+}, Nd^{3+} Phosphor. *J. Alloys Compd.* **2015**, *649*, 62−66.
(34) Bai, B.; Dang, P.; Zhu, Z.; Lian, H.; Lin, J. Broadband Near-Infrared Emission of $La_3Ga_5GeO_{14}$:Tb^{3+},Cr^{3+} phosphors: Energy Transfer, Persistent Luminescence and Application in NIR Light-Emitting Diodes. *J. Mater. Chem. C* **2020**, *8* (34), 11760−11770.
(35) Ye, S.; Song, E. H.; Ma, E.; Zhang, S. J.; Wang, J.; Chen, X. Y.; Zhang, Q. Y.; Qiu, J. R. Broadband Cr^{3+}-Sensitized Upconversion Luminescence in $La_3Ga_5GeO_{14}$: Cr^{3+},Yb^{3+},Er^{3+}. *Opt. Mater. Express* **2014**, *4* (4), 638.

https://doi.org/10.1021/acsaom.2c00198
ACS Appl. Opt. Mater. XXXX, XXX, XXX−XXX